ACCOMMODATING MR DAMPER DYNAMICS FOR CONTROL OF LARGE SCALE STRUCTURAL SYSTEMS

A. Friedman
Purdue University, West Lafayette, IN USA
afriedman@purdue.edu

B. Phillips
The University of Illinois – Urbana Champaign, Champaign, IL USA
bphilli2@uiuc.edu

Z. Jiang
The University of Connecticut, Storrs, CT USA
zhaoshuo.jiang@uconn.edu

S.J. Dyke
Purdue University, West Lafayette, IN USA
sdyke@purdue.edu

B.F. Spencer
The University of Illinois – Urbana Champaign, Champaign, IL USA
bfs@uiuc.edu

R.E. Christenson
The University of Connecticut, Storrs, CT USA
rchriste@uconn.edu

J. Zhang
City College of New York, New York City, NY USA
jzhang13@ccny.cuny.edu

Y. Cha
City College of New York, New York City, NY USA
youngjin.cha@gmail.com

A. Agrawal
City College of New York, New York City, NY USA
agrawal@ccny.cuny.edu

J. Ricles
Lehigh University, Bethlehem, PA USA
jmr5@lehigh.edu

R. Sause
Lehigh University, Bethlehem, PA USA
rs0c@lehigh.edu

Abstract

The focus of this paper is to propose three new control strategies for an advanced damping system utilizing magnetorheological (MR) dampers and investigate their effectiveness, and to validate real-time hybrid testing (RTHT) using an MR damper and the proposed controllers. The first proposed controller, Over-Driven Clipped Optimal Control (ODCOC), combines a clipped-optimal control with over-driven and back-driven current control. The second proposed controller, a displacement feedback-based simple passive controller, is proposed to reduce the computational and sensing cost for seismic mitigation. The third proposed controller is a polynomial-based strategy for semi-active control. Using genetic algorithms, the coefficients of a 4th order polynomial equations about velocity and displacement responses are determined for the best control efficiency. Using an illustrative numerical example, a four story prototype structure equipped with MR dampers is used to evaluate the performance of the proposed control algorithms, compared to alternative control strategies (including clipped-optimal control and others). Via simulations of the structure using various seismic ground motions, reductions in various parameters are examined and compared for all control algorithms. The second part of the study focuses on a RTHT involving the MR damper as an experimental substructure, and the prototype structure designated as the analytical substructure. After performing the RTHT for a suite of controllers using one ground motion, a comparison is made between the results of the numerical simulation performed earlier and the results from the RTHT. The studies discussed herein demonstrate that the proposed control strategies are effective at optimizing damper and structural performance and practically implementable for active and semi-active structural control applications. In addition, the RTHT strategy is validated as an effective method of testing, based upon a response comparison.

Introduction

In the wake of the recent seismic disasters around the world, it is becoming paramount that civil engineers develop a more complete understanding of the effects of earthquakes on structures. On May 12, 2008, at 2:28 PM (CST), an earthquake of magnitude 7.9 struck the Sichuan province in China. The death toll from this event was estimated to be nearly 70,000, and nearly 4,800,000 people were displaced from their homes as a result of the quake. The total losses attributed to the event and recovery were estimated to be in excess $140 billion. Recently, Port-au-Prince, Haiti was devastated by a magnitude 7.0 earthquake. The quake killed over 100,000 people and left more than 1 million homeless, according to preliminary estimates. More than 60,000 were injured, and survivors were in desperate need of medical care, food, water and shelter. The total damage loss was about $5.5 billion, in addition to a daily production loss of $111 million.

These events, as well as many others, have shown the susceptibility of civil infrastructure worldwide to seismic events and led to costly recovery efforts. Advances in technology and materials have paved the way for smarter buildings that can withstand these events. One of the more promising devices for use in structural hazard mitigation is the magnetorheological (MR) damper. MR dampers are adaptable and reliable semi-active devices, which have a large force capacity but require low power levels to achieve them. They possess a large dynamic range and have been shown to be an attractive means of protection for structural systems against severe earthquake loading. In addition, with the controllable-yield stress of MR fluid, MR dampers provide many possible control-based applications. Several effective semi-active control strategies have been developed during recent decades (Dyke et al., 1996; Yi et al., 2001; Choi et al., 2004; Du et al., 2005. Applications of advanced damping systems comprised of these devices and proper control algorithms are expected to facilitate major advances in our ability to achieve performance-based design of structures.

In addition to advanced materials and technology, sophisticated experimental techniques are emerging to validate these concepts and applications. One such method that is gaining traction in the experimental community is real-time hybrid testing (RTHT). RTHT is based on the concept of separating a structure into experimental substructures and analytical substructures. The experimental substructures are tested physically, while the analytical substructures are modeled computationally, with both sides interfacing with each other during an experimental procedure. There are several advantages to this type of testing, including reduced costs as a result of not requiring full-scale models to test structures, not requiring high fidelity models for components that may be quite difficult to effectively model (i.e. highly non-linear devices, etc.), and the ability to effectively capture the behavior of rate-dependant devices. The real-time scale of input presents challenges, specifically the development and implementation of proper actuator delay compensation techniques and robust integration algorithms to maintain the stability of the system. Several integration schemes have been proposed, both implicit (Bonnet et al. 2007, Wu et al. 2005, Nakashima et al. 1992) and explicit (Shing 2002, Cheng and Ricles 2008). Several methods have also been proposed to address the issue of delay compensation (Carrion et al. 2006, Wallace et al. 2005).

The focus of this study is two-fold. In the first part of the study, three new control methods are proposed, implemented in a numerical simulation, and evaluated based on structural responses from four ground motions using specified criteria. The proposed controllers include an over-driven clipped-optimal controller (ODCOC), a displacement-based simple passive controller (SDP), and a displacement- and velocity-based polynomial controller (DVPC). The second part of the study focuses on validating a real-time hybrid test (RTHT) for these proposed controllers. In the RTHT, the MR damper functions as the physical specimen, while the four story prototype structure is modeled computationally. The results of the RTHT are compared to the corresponding numerical simulation.

Problem Formulation

Prototype Structure

The 4-story structure chosen for this control study was designed by the authors from Lehigh University in Bethlehem, PA. It has not been constructed, but it does meet seismic code and is meant to exemplify a typical office building set upon stiff soil in Los Angeles, CA.

The prototype structure (PS) is 64.0 m (210 ft) by 64.0 m (210 ft) in plan, and 16 m (52.5 ft) in elevation. The bays are 9.14 m (30 ft) on center, in both directions, with 7 bays in the E-W direction and 7 bays in the N-S direction. Lateral load resistance is achieved via dual perimeter steel moment-resisting frames (MRF's) on each building face. The interior bays contain simple framing and composite floors. The levels of the PS are numbered with respect to the base story, which is located at the ground level. The fifth story is designated as the roof. The PS has an additional basement level, which is designated as B-1. Typical story heights (for analysis purposes, measured from center-of-beam to center-of-beam) are 3.81 m (12.5 ft), while the basement height is 2.29 m (7.5 ft) and the first story height is 4.57 m (15 ft).

The floor systems are assumed to be rigid in the horizontal plane. The inertial effects of the floor slab are assumed to be evenly distributed to the MRFs, and thus, each MRF accounts for one quarter of the seismic weight associated with each floor of the entire structure. Additionally, there are column splices between the 3rd floor and the roof, located 1.9 m (6.25 ft) above the centerline of the beam-to-column joint. Column base connections are modeled as pinned (at the B-1 level) connections firmly fastened to the ground. The foundation walls and surrounding soil are assumed to restrain the base level of the MRF from horizontal displacement.

The effective seismic weight of the structure was determined with the inclusion of various building components, including the floor slabs, metal decking, mechanical/electrical systems elements, steel framing, exterior cladding and interior partitions. The effective seismic weight of the tributary area corresponding to a single MRF for the first, second, and third floors of the structure is 5388 kN, and the seismic weight of the roof for the same area is 3923 kN. The effective seismic weight of the entire portion of the structure corresponding to a single MRF is 20087 kN.

This study focuses on an in-plane analysis of one quarter of the structure under seismic loading. The frame being considered is one of the E-W MRFs. The MRF will be equipped with four MR dampers in the lower right bay. The dampers are assumed to be connected in the same formation, with positive force from the damper being input to node 9 and negative force being input to node 5. Structural responses are considered only in the horizontal plane, and in the E-W direction.

Evaluation Model

An in-plane finite element model is developed for the MRF, based on the description in the previous section. The moment frame is assumed to remain in the linear response region, and so the global response characteristics will be the focus of this study.

The MRF is modeled using 21 nodes connected using 28 structural elements. Elements are used to represent the beams and columns in the MRF, and nodes are located at beam-column connections and column splice locations. Each node has 3 degrees-of-freedom (DOFs): horizontal, vertical, and rotational. In total, the MRF has 63 DOF before applying boundary conditions and model reduction. Each element has a pre-determined length, area, moment of inertia, modulus of elasticity, and density, and the consistent mass and stiffness matrices are assembled based on these properties.

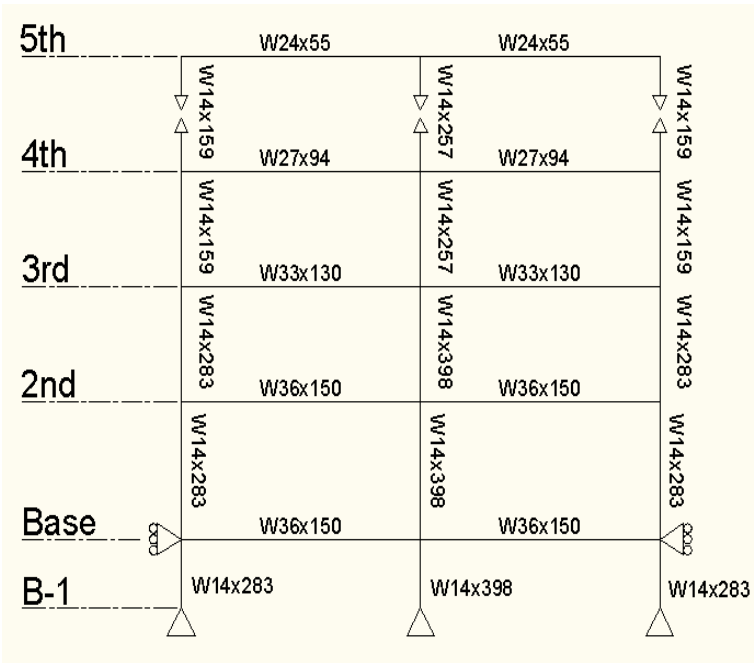

NOTES

f_y = 345 MPa, E = 200 GPa

Restraints
- All columns are pinned at base
- Structure is laterally restrained at base level

Connections
- All connections are moment-resisting

Splices
- Denoted with ▶ ◀
- Occur between the 4th and 5th floors, at 1.91 m (6.25 ft) above the centerline of the 4th floor

Dimensions
- All measurements are center-to-center
- Basement height 2.29 m (7.5 ft)
- Base level height 4.57 m (15 ft)
- 2nd – 5th level 3.81 m (12.5 ft)

Seismic Weight
- Single MRF in E-W direction
- 2nd – 4th level 5380 kN
- 5th level 3923.4 kN

Figure 1 - Structural Model – Evaluation Details

The global stiffness and mass matrices are constructed using a summation of the mass and stiffness of each element for the entire structure. Three separate model reductions were performed on the FE model. The first reduction concerns the boundary conditions of the MRF. In this case, 8 DOFs (five horizontal DOFs and three vertical DOFs) were constrained by eliminating the corresponding row and columns in the global mass and stiffness matrices. The next reduction occurs due to assumption of rigidity of the floor slab in the horizontal plane. These DOFs (eight horizontal DOFs) are constrained by relating the dependent (slave) horizontal DOFs to a single active horizontal DOF in each floor slab and using a Ritz transformation. The last reduction is intended is to eliminate the higher modes and corresponding natural frequencies that do not contribute significantly to the physical response of the structure but can be computationally burdensome. These frequencies can be attributed mostly to the vertical and rotational DOFs, and these will be constrained using partitions for active and slave nodes and a Guyan reduction. The eight horizontal DOFs and five vertical DOFs are designated the active nodes, yielding a 13DOF reduced order model.

A state-space representation of the input-output model of the prototype structure is given by

$$\dot{x} = Ax + Bf + E\ddot{x}_g \tag{1}$$

$$y_m = C_m x + D_m f + F_m \ddot{x}_g + v \tag{2}$$

$$y_e = C_e x + D_e f + F_e \ddot{x}_g \tag{3}$$

$$y_c = C_c x + D_c f + F_c \ddot{x}_g \tag{4}$$

where x is the state vector, y_m is the vector corresponding to the measured outputs, y_e is the vector corresponding to the outputs used for evaluation, and y_c is the vector corresponding to the outputs that are used in control device models. The state space matrices of the system are given as

$$A = \begin{bmatrix} 0 & I \\ -M^{-1}K & -M^{-1}C \end{bmatrix},\ B = \begin{bmatrix} 0 \\ -M^{-1}P \end{bmatrix},\ \mathrm{E} = \begin{bmatrix} 0 \\ -M^{-1}G \end{bmatrix} \tag{5}$$

where $\boldsymbol{M}$, $\boldsymbol{K}$, and $\boldsymbol{C}$ are the mass, stiffness and damping matrices after DOF condensations (Boundary Condition, Ritz, and Guyan) and $\boldsymbol{C_m}$, $\boldsymbol{C_e}$, $\boldsymbol{C_c}$, $\boldsymbol{D_m}$, $\boldsymbol{D_e}$, $\boldsymbol{D_c}$, $\boldsymbol{F_m}$, $\boldsymbol{F_e}$, and $\boldsymbol{F_c}$ are appropriate matrices corresponding to the chosen output vectors.

The model is assumed to be a pre-earthquake model that represents the as-built structure. As such, the stiffness of the structure is supplemented by the lateral resistance of the structures gravity system and non-structural elements like partitions and cladding. These elements are accounted for in the model by multiplying the stiffness matrix by 1.21 (equivalent to proportionally increasing the natural frequency of the structure by 10%). The damping matrix is determined using this increased stiffness matrix.

The natural frequencies for the structural model are 0.70 1.82 3.36 5.22 5.36 7.12 8.12 18.11 19.88 34.98 41.61 62.27 and 316.07 Hz, and this model is used to evaluate the proposed control strategies, based on the criteria as described in a later section.

The Magnetorheological Damper Model

This study used a 200-kN MR damper developed by the Lord Corporation. A schematic of the large-scale MR damper is shown in Figure 2. The damper is 1.47 m (58 inches) in length, weighs approximately 2.734 kN (615 lbs), and has an available stroke of 584 mm (23 inches). The damper's accumulator can accommodate a temperature change in the fluid of 80°F. The damper can provide control forces of just over 200 kN (45 kip).

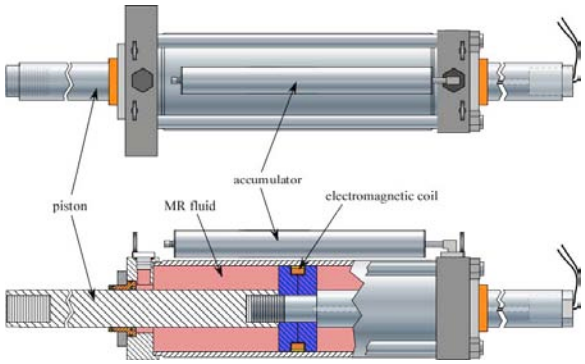

Figure 2 - Large-scale Semi-active Damper Schematic

The MR damper is controlled with a low voltage, current driven command signal. The coil resistance is approximately 4.8 Ohms, while the inductance is approximately 5 H at 1 amp and 3 H at 2 amps. An Advanced Motion Controls PWM Servo-Amplifier (30A8DDE) is powered by an 80 volt DC, 5 amp unregulated linear power supply. The servo-amplifier is used to provide the command signal that controls the electromagnetic field for each damper. The PWM Servo-Amplifier is controlled by a 0-5 volt DC signal and utilizes pulse width modulation for current control. The input control signal can be switched at a rate of up to 1 kHz, although the rise time of the current signal is limited by the inductance of the MR damper. Each damper has been fitted with a 1.5KE75A transient voltage suppressor to protect the MR damper electromagnetic coils from unintended and damaging voltage peaks.

There are many proposed models for MR dampers (Jiang et al., 2010). For this study, a model was developed for the 200 kN MR damper based on a phenomenological Bouc Wen model (Dyke et al., 1997), which is characterized by the following equations:

$$c_1\dot{y} = \alpha z + k_0(x_d - y) + c_0(\dot{x}_d - \dot{y}) \quad (6)$$

$$\dot{z} = -\gamma|\dot{x}_d - \dot{y}|z|z|^{n-1} - \beta(\dot{x}_d - \dot{y})|z|^n + A(\dot{x}_d - \dot{y}) \quad (7)$$

$$f = \alpha z + c_0(\dot{x}_d - \dot{y}) + k_0(x_d - y) + k_1(x_d - x_0) \quad (8)$$

where f represents the damper force, k_1 represents the accumulator stiffness, c_0 represents the viscous damping observed at large velocities, c_1 (represented here as a dashpot in the model) is included to produce the roll-off observed at low velocities, k_0 represents the stiffness at large velocities, and x_0 is the initial displacement of the spring k_1 associated with the nominal damper force due to the accumulator.

Using the ATLSS Lab facilities at Lehigh University and Smart Structures Technology Laboratory facilities at the University of Illinois-Urbana/Champaign, a series of tests were conducted to measure the damper response under various loading conditions, in an effort to characterize a model for the damper. At Lehigh, the MR damper (as previously described) was attached to a 517 kip actuator. At UIUC, the MR damper was attached to a 125 kip Shore Western. hydraulic actuator. In each test, the actuator was driven with a sinusoidal input signal, having a fixed amplitude and frequency, while the voltage being input to the MR damper was also constant. A wide range of frequencies and voltage values were selected for testing.

To achieve optimal performance, the damper model must be able to account for fluctuating current levels based on the response of the structural system to which it is attached. To establish a model which accounts for fluctuating magnetic fields, the relationships of the parameters to the current must be determined. Based upon the initial damper tests, the relationships for α and c_0 were determined to be exponential in nature, while c_1 was taken to be an irrational expression. These relationships are proposed as

$$\alpha = \alpha_A e^{(\alpha_B i)} + \alpha_C e^{(\alpha_D i)} \quad (9)$$

$$c_o = c_{0A} e^{(c_{0B} i)} + c_{0C} e^{(c_{0D} i)} \quad (10)$$

$$c_1 = c_{1A}\sqrt{i} + c_{1B} \quad (11)$$

where i is the current applied to damper from the current driver. In total, optimal values of 17 parameters ($\alpha_A\ \alpha_B\ \alpha_C\ \alpha_D\ c_{0A}\ c_{0B}\ c_{0C}\ c_{0D}\ c_{1A}\ c_{1B}\ k_0\ k_1\ x_0\ \beta\ \gamma\ n\ A$) must be determined to model the MR damper.

These parameters were determined using a constrained non-linear optimization. The optimization was performed using the curve fit tool available in MATLAB (2009). Table 1 provides these optimized parameters for the generalized model.

Phenomenological Bouc Wen Model Parameters			
Parameter	**Value**	**Parameter**	**Value**
α_A	950.4 kN	c_{1A}	100 kNsec/m
α_B	-0.0098 kN	c_{1B}	28470 kNsec/m
α_C	-934.3 kN	k_0	0.0559 kN/m
α_D	0.9376 kN	k_1	0.0641 kN/m
c_{0A}	277.4 kNsec/m	x_0	0.01 m
c_{0B}	-0.0012 kNsec/m	β	4430 m^{-1}
c_{0C}	-184.4 kNsec/m	γ	4430 m^{-1}
c_{0D}	-1.13 kNsec/m	A	336.56
		n	2

Table 1 – MR Damper Model Parameters

Control Design

Over-Driven Clipped Optimal Control

The first proposed control algorithm is Over-Driven Clipped Optimal Control (ODCOC). ODCOC combines the concepts of a clipped optimal controller with the effects of over- and back-driven current control. The ODCOC utilizes a force feedback loop appended to a seismically excited structure equipped with MR dampers. Based on the measured acceleration outputs of the system and the measured forces of the dampers, a state-space linear quadratic Gaussian (LQG) regulator is designed to provide the desired control force, f_{DES}. This regulator is coupled with a control law designed to select the appropriate voltage value to induce the damper to reach the desired force. The control law incorporates the concepts of over- and back-driving the damper into the method for selecting the voltage. Both over- and back-driving the MR damper are techniques used to significantly improve the damper response and thus increase the mitigation of seismic effects in the structure. Given the nature of the MR fluid inside of the damper, there is a time delay between the voltage commanded to the MR damper and the damper achieving the force response associated with that voltage level. By initially commanding a higher voltage level (or over-driving the damper) and then lowering the voltage level once the desired force level has been attained, the response time of the damper can be lowered and better performance can be achieved. In this case, when over-driving the MR damper, an amplified voltage level of 7.5 volts is applied to the damper until it reaches the desired force level, and then the voltage level is set to 2.5 volts. The technique is similar on the down side of the force (when f_{DES} is trending toward zero). There is a time delay (due to the dissipation of the magnetic field generated by the damper) between the voltage commanded and the force reduction achieved by the damper. By applying a voltage of -7.5 volts when the MR damper force is not dissipative (i.e. f_{DES} and f_{MEAS} have different signs), the magnetic fields generated by the MR damper can be forcibly reduced, thereby breaking the magnetic bonds between the iron particles in the fluid, and the damper response time can be significantly improved. Once the desired force levels have been realized, or if the force is on the downside and is not dissipative, the voltage level is then set to zero volts.

Because the force generated by a MR damper cannot be directly commanded, a method must be devised to command the voltage, v, to the current driver for the MR damper. The voltage is selected to generate

the approximate desired optimal control force, f_{DES}, in the damper as follows. There are four main variables that form the basis for this control approach, which include: the desired force, f_{DES}; the measured force, f_{MEAS}; the maximum force capacity of the damper, f_{MAX}; and the smallest force capacity of the damper (defined as the minimum force generated by the damper in an "off" state), f_{MIN}. Control is divided into two distinct regions, which are based upon the sign of the measured force, f_{MEAS}. In the first region, when f_{MEAS} has a positive value, the possible voltage levels are 2.5 and 7.5 volts. If f_{MEAS} is greater than f_{DES} and f_{MEAS} is less than f_{MAX}, the voltage is set to 7.5 volts. If f_{MEAS} is greater than f_{MAX}, the voltage is set to 2.5 volts. In the alternative region, when f_{MEAS} has a negative value, the possible voltage levels are -7.5 and zero volts. If f_{MEAS} is greater than or equal to f_{DES} and f_{MIN}, and f_{MEAS} and f_{DES} have different signs, then the voltage is set to -7.5 volts. If f_{MEAS} is greater than or equal to f_{DES}, but f_{MEAS} and f_{DES} have the same signs, or if f_{MEAS} is greater than or equal to f_{DES}, f_{MEAS} and f_{DES} have different signs, but f_{MEAS} is less than $f_{MIN,}$ then the voltage level is set to zero volts. This control algorithm is shown visually in Figure 3.

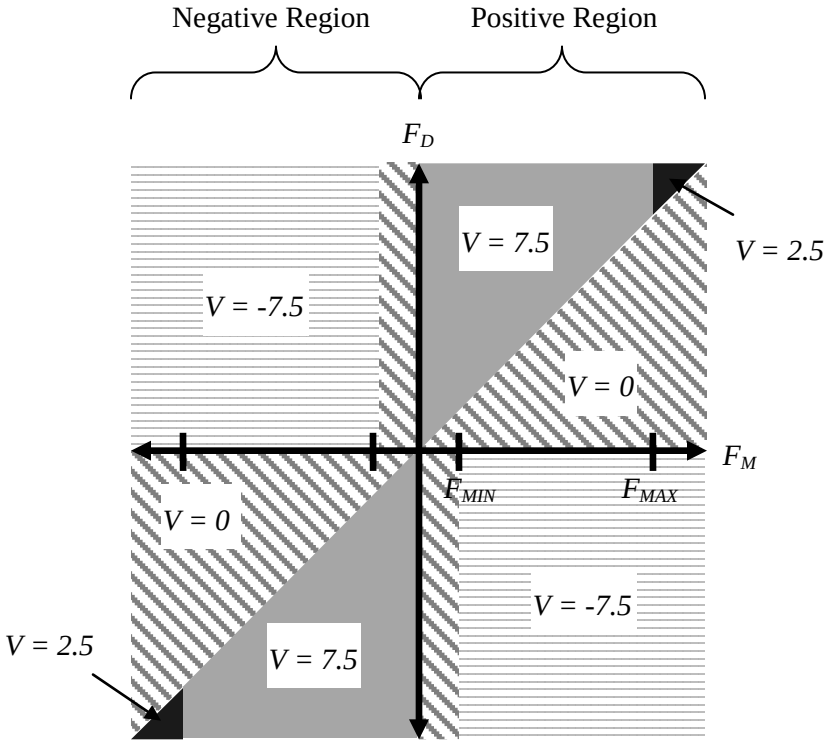

Figure 3 - Visual Representation of Over-Driven Clipped Optimal Control Law

Simple Passive Control

The second proposed controller is a simple displacement-based passive controller (SDP). Consider a MR damper horizontally installed between two stories of a seismic excited building, the force generated by the MR damper is determined by interstory displacement, interstory velocity and voltage input to the damper. Moreover, experiment shows that MR dampers generate large forces when both the input velocity and voltage are large.

Due to the fact that the force generated by MR damper is a function of input displacement, velocity and voltage, the output force cannot merely be commended by the voltage. The approach proposed here tries to utilize the high interstory velocity when the building vibrates across its original position; simultaneously, a high voltage will be input to the MR damper to help generate a large control force.

Therefore, during the vibration of a damped structure, a relatively large control force will be generated to "catch" the structure when it passes by its original position.

One disadvantage of a passive system is that it results in a larger acceleration than the semi-active and passive-off systems, since the passive-on system attempts to lock-up and increase the absolute acceleration of the damped floors, and also increase the drifts of the undamped floors (Jansen et al., 2000). To avoid the lock-up problem, the voltage from the simple passive controller will decrease to zero when the floor swings away from its original position, and the dropping-off of the control voltage is designed in a ramp pattern to avoid a sudden change in the control force. The control rule can be graphically represented as in Eqn. 1, and the voltage from the controller is

$$V = \begin{cases} Vmax & |x| < x_0 \\ \frac{Vmax}{x_1}(x_0 + x_1 - |x|) & x_0 \le |x| \le x_0 + x_1 \\ 0 & |x| \ge x_0 + x_1 \end{cases} \quad (12)$$

where x is the interstory displacement of the floor on which the MR damper is installed; x_0 , x_1 and $Vmax$ are the parameters that need to be determined by designers.

The simple feature of this passive controller makes it easy to be realized by simple mechanical and electrical devices. Figure 4 shows a passive control system that integrates both the MR damper and the simple passive controller. The pin moves together with the piston of the MR damper; the electrical

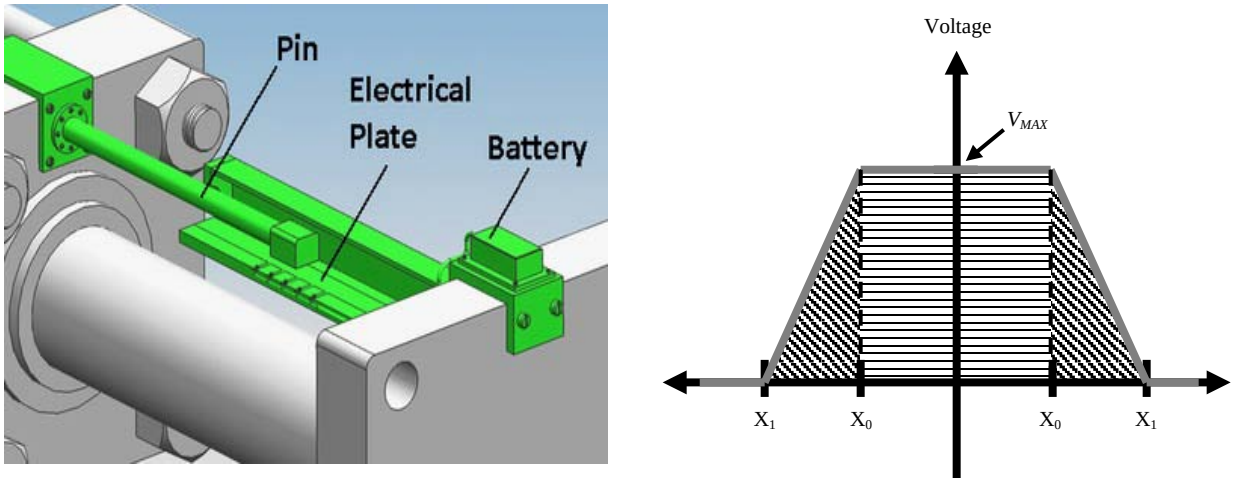

Figure 4 – Concept of the Simple Passive Controller

plate is fixed to the damped floor or the enclosure of MR damper. When the piston moves, the tip end of the pin contacting with the electrical plate is capable to feedback the control voltage to the amplifier. The voltage on the electrical plate along the direction of stroke is regulated according to the chosen design parameters.

The simple passive controller, which is operates on battery power, is shown in Figure 4. It consists of a pin fixed to the MR damper enclosure, an electrical plate attached to the piston of the MR damper and a battery cage. As shown, the system integrates the displacement sensor and a simple passive controller together.

Displacement- and Velocity-Based Polynomial Control

The third proposed controller is a polynomial control algorithm (DVPC) for semi-active control device. This novel polynomial controller consists of polynomial equations that express the relationships between structural responses and optimal current for the MR dampers. Two types of novel polynomial controller are possible as semi-active control algorithm. The first design is that the one polynomial equation expressing the relationship between displacement and control signal is used. The second one is that two polynomial equations expressing the relationship among the displacement and velocity and control signal are used. The control signal (v) function, composed of 4th order polynomial coefficients, is expressed as

$$\mathrm{v} = |a_1 x^3 + a_2 x^2 + a_3 x + a_4| \tag{13}$$

where x is the interstory drift and $a_1 \sim a_4$ are the optimal coefficients of polynomial equation for the control system. The displacement and velocity based control signal, v, is expressed as

$$v = |a_1 x^3 + a_2 x^2 + a_3 x + a_4| + |b_1 \dot{x}^3 + b_2 \dot{x}^2 + b_3 \dot{x} + b_4| \tag{14}$$

where $\dot{x}$ is the interstory velocity and $a_1 \sim a_4$, and $b_1 \sim b_4$ are optimal coefficient of polynomial equation for control system and v should have maximum and minimum limitation dependant on the MR damper size.

The coefficients of the polynomial equations can be found using optimization search method. In this case, implicit redundant representation genetic algorithm (IRR GA) was used to find the optimal coefficients of the 4th order polynomial equations for the 4 story prototype building. To get a reliable controller, diverse strengths and type of earthquakes were used in this optimization search method.

Real-Time Hybrid Testing & Validation

Test Setup for Real-Time Hybrid Simulation

The second focus of this study is the implementation and validation of the proposed controllers in a real-time hybrid test (RTHT). The PS-MR damper structural system will be divided into an experimental substructure (the MR damper) and an analytical substructure (the MRF). The MR damper will be physically excited by a hydraulic actuator, while the MRF will be modeled computationally for the duration of the experiment. Using the equipment as described below, various controllers can be tested with the structural system for a single, specific earthquake motion. A schematic of the real-time hybrid test is shown below in Figure 5.

The RTHT was conducted at the University of Illinois – Urbana/Champaign (Phillips et al., 2010). The real-time hybrid testing framework at the University of Illinois is located in the Newmark Structural Engineering Laboratory and is a part of the Smart Structures Technology Laboratory. The actuator responsible for excitation is a Shore Western Corporation 125 kips hydraulic actuator, with a maximum stroke of ± 152.4 mm (6 in) and an effective piston area of 271 cm^2 (42 in^2). A three-stage servo-valve is used to control the actuator, consisting of a Schenck-Pegasus model 1800 rated at 80 gpm and a Schenck-Pegasus model 20B two-stage servo-valve rated at 0.86 gpm The displacement of the actuator is measured using an internal AC LVDT. A 100 kip Schenck-Pegasus load cell in line with the actuator measures the restoring force of the attached specimen. The actuator and specimen (MR damper) are both mounted on a 7.62 (3 in) thick steel plate. Steel blocks and wedges are used to prevent lateral translation of the actuator and specimen. The equipment listed above has previously proven successful for the dynamic testing of large-scale MR dampers (Yang, 2001).

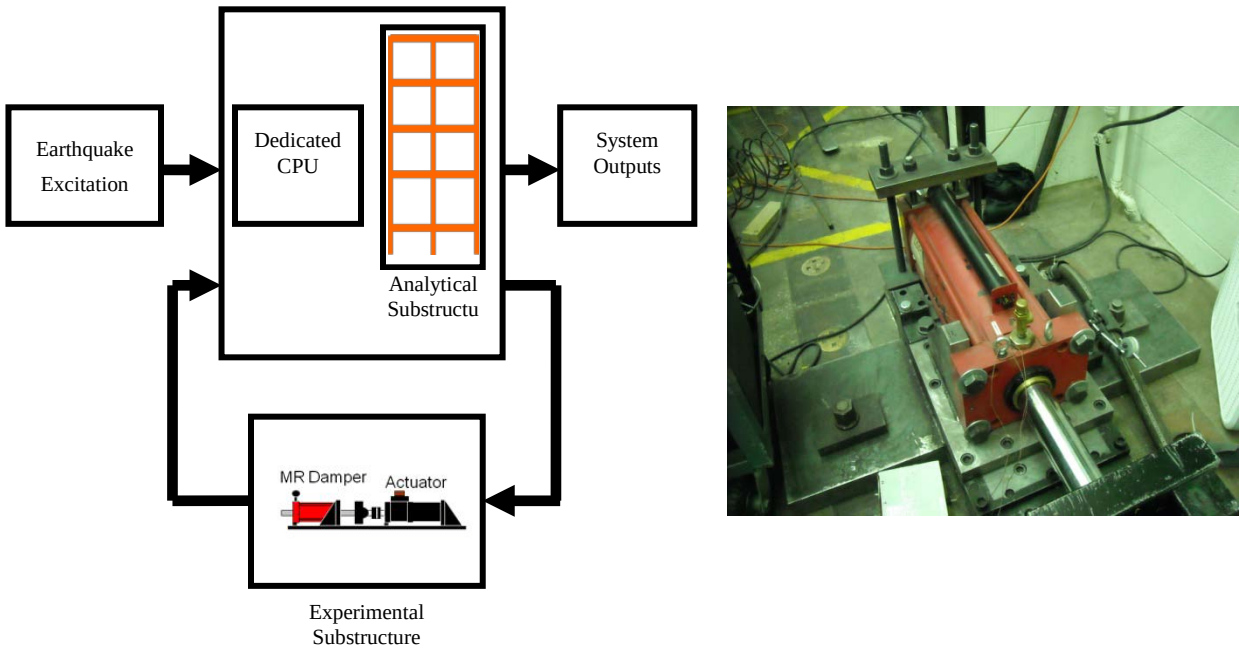

Figure 5 - Real Time Hybrid Testing Diagram/Setup

The integrated hardware in the RTH framework consists of a Shore Western model 1104 digital servo-controller which accepts externally generated commands from a dSPACE model 1103 digital signal processing (DSP) board. This board is used to perform numerical integration of the equations of motion for the numerical substructure, employ the real-time hybrid simulation delay compensation techniques on outgoing commands, and compute the desired current for the MR damper based on semi-active control laws. These three numerical components are programmed on a host computer using Simulink, a block diagram style programming tool within MATLAB. The Simulink model is translated to C-code using Real Time Workshop and transferred to the DSP board. Real-time execution of the code is controlled and monitored from the host computer. The host computer also acts at the DAQ, logging data from specified channels within the Simulink model.

Numerical and Hybrid Results

Numerical Simulations

To evaluate the effectiveness of the proposed controllers, several input excitations, $\ddot{x}_g$, were used in simulation: (i) *El Centro.* (ii) *SAC Small Earthquake.* (iii) *SAC Medium Earthquake* (iv) *SAC Large Earthquake.* Each control strategy is evaluated for each seismic input, with the appropriate measured outputs being used to calculate the various evaluation criteria. As described in the following page, the evaluation criteria are based upon maximum response characteristics, and in general, smaller values for the evaluation criteria are indicative of better performance (Spencer et al., 1999).

The results for each earthquake excitation, with each controller, are shown below.

J Value	Equation	Description	J Value	Equation	Description
$\mathbf{J_1}$	$\max_{\substack{El\ Centro \\ SAC\ Large \\ SAC\ Medium \\ SAC\ Small}} \left\{ \frac{\max_{t \quad i\in\eta} \lvert x_i(t) \rvert}{x^{max}} \right\}$	Floor Displacement Ratio of controlled maximum relative displacement to the uncontrolled value	$\mathbf{J_6}$	$\max_{\substack{El\ Centro \\ SAC\ Large \\ SAC\ Medium \\ SAC\ Small}} \left\{ \frac{\max_{t,i} \frac{\lVert d_i(t) \rVert}{h_i}}{\lVert d_n^{max} \rVert} \right\}$	Normed Interstory Drift Ratio of controlled maximum normalized interstory drift to the uncontrolled value
$\mathbf{J_2}$	$\max_{\substack{El\ Centro \\ SAC\ Large \\ SAC\ Medium \\ SAC\ Small}} \left\{ \frac{\max_{t,i} \frac{\lvert d_i(t) \rvert}{h_i}}{d_n^{max}} \right\}$	Interstory Drift Ratio of controlled maximum interstory drift to the uncontrolled value	$\mathbf{J_7}$	$\max_{\substack{El\ Centro \\ SAC\ Large \\ SAC\ Medium \\ SAC\ Small}} \left\{ \frac{\max_{t,i} \frac{\lVert \ddot{x}_{ai}(t) \rVert}{h_i}}{\lVert \ddot{x}_a^{max} \rVert} \right\}$	Normed Floor Acceleration Ratio of controlled maximum normalized floor acceleration to the uncontrolled value
$\mathbf{J_3}$	$\max_{\substack{El\ Centro \\ SAC\ Large \\ SAC\ Medium \\ SAC\ Small}} \left\{ \frac{\max_{t \quad i\in\eta} \lvert \ddot{x}_{ai}(t) \rvert}{\ddot{x}_a^{max}} \right\}$	Floor Acceleration Ratio of controlled maximum absolute acceleration to the uncontrolled value	$\mathbf{J_8}$	$\max_{\substack{El\ Centro \\ SAC\ Large \\ SAC\ Medium \\ SAC\ Small}} \left\{ \frac{\left\lVert \sum_{i=1}^{4} m_i x_{a\eta i}(t) \right\rVert}{\lVert F_b^{max} \rVert} \right\}$	Normed Base Shear Ratio of controlled maximum normalized base shear to the uncontrolled value
$\mathbf{J_4}$	$\max_{\substack{El\ Centro \\ SAC\ Large \\ SAC\ Medium \\ SAC\ Small}} \left\{ \frac{\max_{t} \lvert \sum_{i=1}^{4} m_i x_{a\eta i}(t) \rvert}{F_b^{max}} \right\}$	Base Shear Ratio of controlled maximum base shear to the uncontrolled value	$\mathbf{J_9}$	$\max_{\substack{El\ Centro \\ SAC\ Large \\ SAC\ Medium \\ SAC\ Small}} \left\{ \frac{\max_{t,i} \lvert f^i(t) \rvert}{W} \right\}$	Control Force Ratio of the maximum device output force to the weight of the structure
$\mathbf{J_5}$	$\max_{\substack{El\ Centro \\ SAC\ Large \\ SAC\ Medium \\ SAC\ Small}} \left\{ \frac{\max_{i\in\eta} \lVert x_i(t) \rVert}{\lVert x^{max} \rVert} \right\}$	Normed Floor Displacement Ratio of controlled maximum normalized relative displacement to the uncontrolled value	$\mathbf{J_{10}}$	$\max_{\substack{El\ Centro \\ SAC\ Large \\ SAC\ Medium \\ SAC\ Small}} \left\{ \frac{\max_{t,i} \lvert y_i^a(t) \rvert}{x^{max}} \right\}$	Control Device Stroke Ratio of the maximum stroke of the control device to the uncontrolled displacement of the structure.

J values	Passive Off	Passive On	COC	ODCOC	SPC	DVPC
El Centro Earthquake Ground Motion						
J_1	0.934	0.757	0.736	0.754	0.766	0.753
J_2	0.972	0.748	0.762	0.736	0.765	0.738
J_3	0.971	0.757	0.775	0.746	0.772	0.748
J_4	0.943	0.829	0.787	0.829	0.820	0.825
J_5	0.920	0.529	0.548	0.528	0.544	0.530
J_6	0.922	0.576	0.582	0.574	0.593	0.573
J_7	0.924	0.616	0.625	0.615	0.640	0.613
J_8	0.918	0.555	0.568	0.555	0.574	0.555
J_9	0.001	0.010	0.010	0.011	0.010	0.011
J_{10}	0.329	0.253	0.258	0.249	0.259	0.250
SAC Large Earthquake Ground Motion						
J_1	0.949	0.702	0.718	0.692	0.708	0.697
J_2	0.948	0.707	0.728	0.697	0.717	0.701
J_3	0.944	0.834	0.836	0.833	0.854	0.832
J_4	0.957	0.765	0.784	0.757	0.766	0.760
J_5	0.900	0.384	0.435	0.367	0.416	0.377
J_6	0.902	0.413	0.454	0.399	0.443	0.405
J_7	0.911	0.502	0.537	0.488	0.530	0.494
J_8	0.902	0.421	0.464	0.404	0.452	0.412
J_9	0.002	0.014	0.013	0.014	0.013	0.015
J_{10}	0.326	0.243	0.251	0.240	0.247	0.241
SAC Medium Earthquake Ground Motion						
J_1	0.983	0.878	0.888	0.873	0.915	0.877
J_2	0.983	0.880	0.890	0.875	0.919	0.878
J_3	0.985	0.903	0.912	0.900	0.941	0.903
J_4	0.972	0.859	0.868	0.855	0.905	0.858
J_5	0.934	0.685	0.714	0.683	0.808	0.689
J_6	0.935	0.692	0.720	0.690	0.815	0.696
J_7	0.939	0.717	0.744	0.716	0.830	0.720
J_8	0.933	0.684	0.713	0.683	0.809	0.688
J_9	0.004	0.019	0.016	0.018	0.012	0.019
J_{10}	0.303	0.271	0.274	0.270	0.283	0.271
SAC Small Earthquake Ground Motion						
J_1	0.917	0.602	0.643	0.591	0.602	0.596
J_2	0.952	0.706	0.755	0.698	0.711	0.701
J_3	0.950	0.721	0.769	0.714	0.724	0.716
J_4	0.953	0.641	0.684	0.626	0.646	0.633
J_5	0.923	0.416	0.454	0.426	0.426	0.429
J_6	0.923	0.451	0.477	0.456	0.463	0.458
J_7	0.922	0.498	0.523	0.503	0.512	0.504
J_8	0.922	0.438	0.470	0.445	0.449	0.447
J_9	0.001	0.010	0.009	0.011	0.010	0.011
J_{10}	0.269	0.199	0.213	0.197	0.201	0.198

Table 2 – Numerical Simulation Results

Real Time Hybrid Simulation

To validate the real-time hybrid test approach with the proposed controllers, the results of the numerical simulation from the previous section for the SAC small earthquake excitation were compared to the results of a hybrid simulation using the same controller and earthquake record. Based on the simulation results, the ODCOC was selected as the representative controller.

The results from the real-time hybrid test using the ODCOC compared to the simulation are shown below in Figure 6. Several representative plots are shown here, consisting the 3rd floor displacement, velocity and acceleration for the ODCOC controller. From these graphs, it is clear that the RTHT simulations compare well with the numerical simulation for the ODCOC,

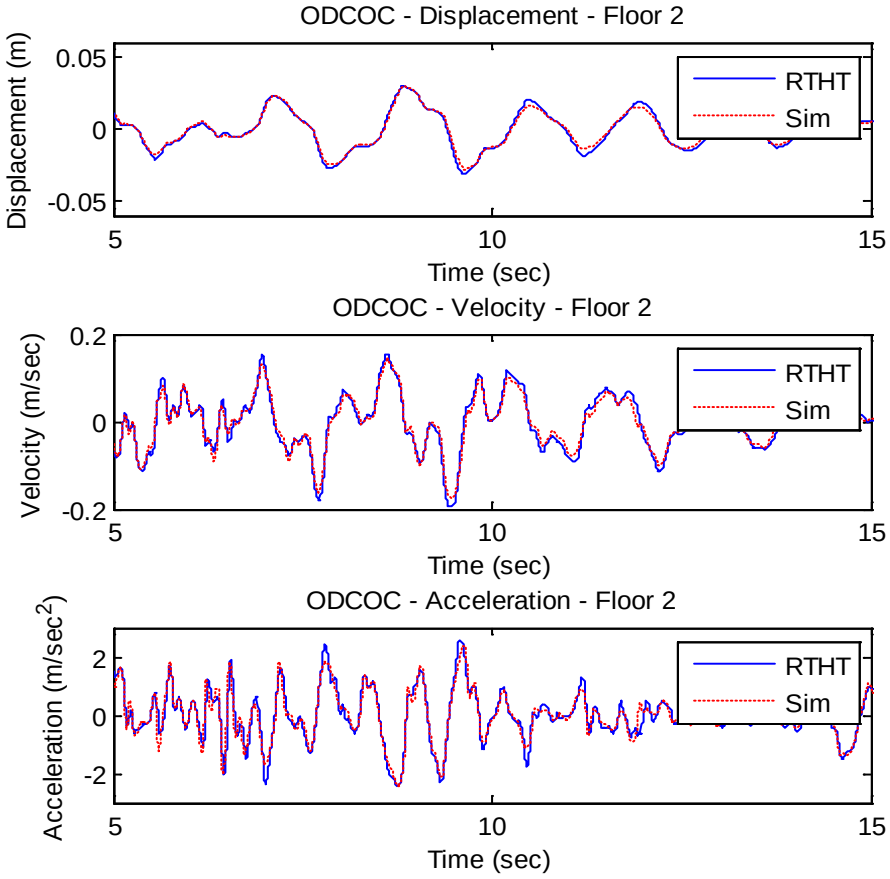

Figure 6 - RTHT Results - ODCOC

Conclusions

In this study we proposed three new control strategies for use in structures equipped with MR dampers. Using a four-story, two-bay prototype structure equipped with four MR dampers in the first story, the control strategies have been implemented and tested using four different earthquake records. Overall, the proposed controllers performed well in reducing the response of the structural system. All of the proposed controllers were able to achieve an approximate 25% reduction in relative displacement for the El Centro earthquake, an approx. 30% reduction for the Large SAC earthquake, an approx. 12% reduction for the Medium SAC earthquake record, and an approx. 40% reduction for the

Small SAC earthquake record. The controllers were able to achieve an approx. 25% reduction in absolute acceleration of the structure for the El Centro earthquake record, an approx. 16% reduction for the Large SAC earthquake record, an approx. 10% reduction for the Medium SAC earthquake record, and an approx. 27% reduction for the Small SAC earthquake record. Due to the size and layout of this particular structure, as expected, marginal improvement was observed over the passive-on controller. The In these tests the ODCOC had the best performance, with an approximately 3% average performance improvement over the standard COC controller. In addition, real-time hybrid simulation was validated for the ODCOC controller. The structural responses were shown to track the numerical simulation results very well.

Future Work

Different structures (including non-linear elements) and damper location scenarios will be used in the future to examine the performance of these controllers on a variety of building types. We anticipate that this examination will demonstrate superiority of these semi-active designs over passive systems. To further validate the real-time hybrid simulations, we will be conducting large-scale frame testing using the NEES facility RTMD at Lehigh University.

Acknowledgements

The authors wish to acknowledge that the funding for this project was provided by CMMI Grant # 1011534.

References

Bonnet P.A., Lim C.N., Williams M.S., Blakeborough A., Neild S.A., Stoten D.P., and Taylor C.A., (2007) "Real-time hybrid experiments with Newmark integration, MCSmd outer-loop control and multi-tasking strategies." *Earthquake Engineering and Structural Dynamics* **36**(1):119–141.

Chen C. and Ricles J., (2008) "Development of Direct Integration Algorithms for Structural Dynamics Using Discrete Control Theory," *Journal of Engineering Mechanics* **134**(8): 676-683

Choi, K.M., Cho, S.W., Jung, H.J., Lee, I.W., (2004) "Semi-active fuzzy control for seismic response reduction using magnetorheological dampers," *Earthquake Engng Struct. Dyn.* 2004; 33:723-736

Du, H., , Sze, K.Y., Lamb, J., (2005) "Semi-active H∞ control of vehicle suspension with magneto-rheological dampers," *Journal of Sound and Vibration*, Volume 283, Issues 3-5, 20 May 2005, Pages 981-996

Dyke, S.J., Spencer, B.F., Jr., Sain, M.K., and Carlson, J.D., (1996) "Modeling and control of magnetorheological dampers for seismic response reduction," *Smart Mater. Struct.* 5 565

Dyke, S.J., Spencer, B.F., Jr., Sain, M.K., and Carlson, J.D., (1997) "Phenomenological Model of a Magnetorheological Damper," *ASCE Journal of Engineering Mechanics* 123(3): 230-238

Jansen, L.M., Dyke, S.J., (2000) "Semi-active control strategies for MR dampers: a comparative study," *Journal of Engineering Mechanics*, Vol. 126, No. 8, August 2000, pp. 795-803

Jiang, Z. et al., (2010) "Comparison of a 200 kN MR Damper models for use in real-time hybrid simulation." *Proc. of the 5th WCSCM*, Tokyo Japan July 12-14 2010

Nakashima M., Kato H., and Takaoka E., (1992) "Development of real-time pseudo dynamic testing." *Earthquake Engineering and Structural Dynamics* **21**(1):79–92.

Phillips, B., et al., (2010) "Real-Time Hybrid Simulation Benchmark Study with a Large-Scale MR Damper." *Proc. of the 5th WCSCM*, Tokyo Japan July 12-14 2010

Shing, P.B., (2002) "Development of high-speed on-line substructuring testing system at the University of Colorado." *CASCADE Technical Workshop*, Oxford, U.K.

Spencer, B.F., Christenson, R.E., and Dyke, S.J. (1999) "Next Generation Benchmark Control Problem for Seismically Excited Buildings," *ASCE Journal of Engineering Mechanics*, 121(2): 322–338

Wu, B., Bao H., Ou J., and Tian S., (2005) "Stability sand accuracy of the central difference method for real-time substructure testing." *Earthquake Engineering and Structural Dynamics* **34**(7):705–718.

Yang, G. (2001), "Large-Scale Testing Magnetorheological Fluid Damper for Vibration Mitigation: Modeling, Testing, and Control," *Dissertation, Univ. of Notre Dame*

Yi, F., Dyke, S.J., Caicedo, J.M., Carlson, J.D., (2001) "Experimental verification of multi input seismic control strategies for smart dampers," *Journal of Engineering Mechanics*, Vol. 127, No. 11, November 2001, pp. 1152-1164